Detecting Alpine Treeline Ecotones – an Automated Remote Sensing Approach

Thesis Paper for the Project Seminar: Treelines of the World in SS 2020

University Lecturer: Dr. Maaike Bader, Physical Geography, Philipps-Universität Marburg

Student: Agnes Schneider

Matriculation number: 2689766

E-Mail: Schnei7v@students.uni-marburg.de; euboia@gmail.com

Date of Submission: 01.01.2022

Abstract

1 Introduction

Alpine Treeline Ecotones (ATEs) are transitional zones between subalpine Forest and Alpine (tundra) ecotones (Holtmeier & Broll (2005), Winings (2013)) also referred to as upper-treeline (Elliott (2017)) and occur globally (Singh et al. (2015), Bader et al. (2021)). They span between the actual Timberline/Economic Forest Line though the Upper/Physiognomic-Biologic Forest Line and the tree species line which is adjoining the actual Alpine zone (Chhetri & Thai (2019), 1543). The position of the treeline is influenced by multiple factors at local and regional level, but temperature has been identified as the global driving factor (Körner (1998), Körner & Paulsen (2004), Holtmeier & Broll (2005), Bader et al. (2007), Barredo Cano et al. (2020)). The global pattern can be described by spatial patterns in the x-y plane (discrete or diffuse, Figure 1) and by changes in tree stature (abrupt or gradual, Figure 2) in a multi-dimensional space (Harsch & Bader (2011), Bader et al. (2021)).

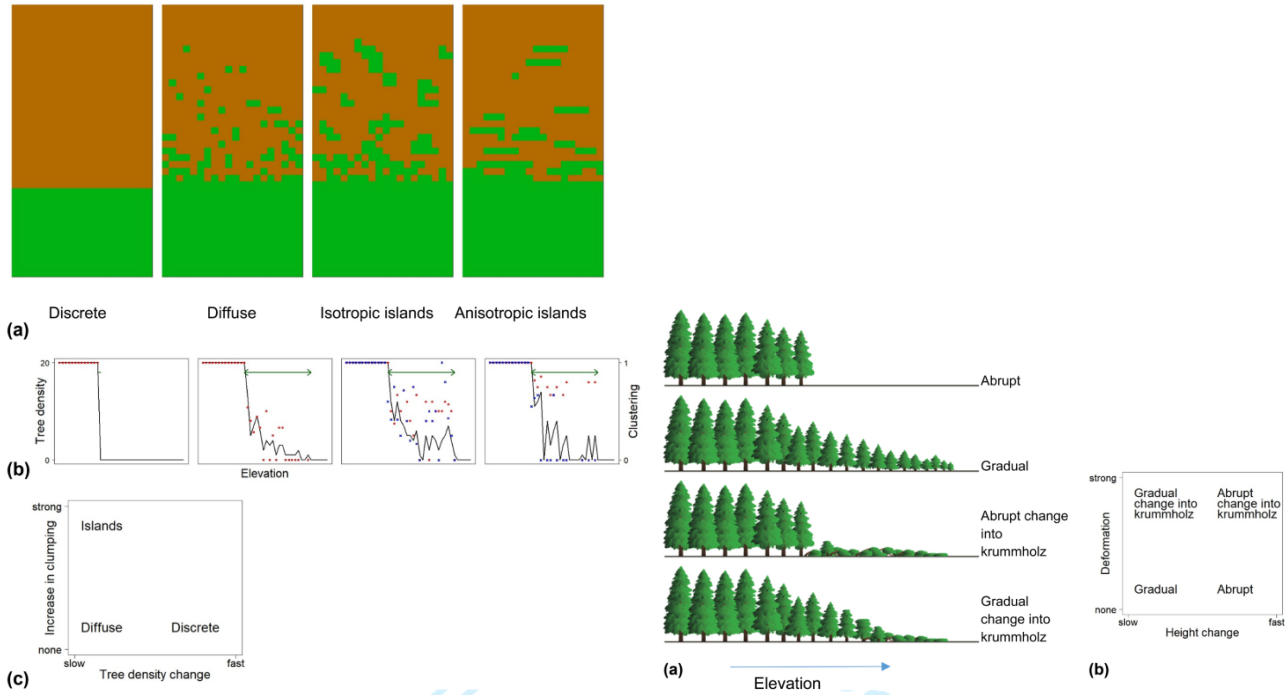

Figure 1: Left: Scheme of the spatial pattern of alpine treelines on the 2D x-y plane. a) Depicts the treeline as seen from above, while b) depicts the change of the treeline in the y direction (clustering of islands). c) Represents an abstraction of the pattern of treelines based on tree density change and the clustering of individual trees. Source: @baderGlobalFrameworkLinking2021, Figure 1. Right: Scheme of (discrete) tree stature/height change responding to change in elevation. a) Vertical cross section. b) Abstraction of tree stature change based on height change and deformation of tree shape. Source: @baderGlobalFrameworkLinking2021, Figure 2.

Although recognized, the distribution of ATE patterns have neither been mapped, nor been

described yet, let alone explained. Earlier studies have identified abrupt, diffuse, island and krummholz spatial patterns of ATEs (Harsch et al. (2009), Harsch & Bader (2011), Figure 2). As seen, treelines dispaly a high variability and differ in multiple dimensions. A comparison of multiple studies suggest, that the different spatial patterns of ATEs reflect fundamental ecological controlling processes and that different ATEs react differently to climate change (Harsch & Bader (2011), Figure 1) Figure 3.

	a) Rate of change	b) Type of change	Controlling processes (first-level)	Controlling processes (second- and third-level)
2-D pattern	**Discrete**		Mortality above but not in the ecotone	Any type of damage or stress. If gradual, growth limitation above the ecotone
	Ecotone	**Diffuse**	Mortality within the ecotone	Environmental heterogeneity or stochasticity. And/or ongoing seed-limited colonization
		Island	Mortality within the ecotone	Positive feedback due to radiation damage, freezing damage, wind damage, snow redistribution (snow moulds, growing-season length), clustered seed dispersal, clonal reproduction
Tree stature	**Abrupt**	Into alpine	Mortality	Overheating, desiccation, photoinhibition, freezing damage, soil limitations
		Into krummholz	Dieback	Winter desiccation, snow moulds, browsing, abrasion
	Gradual	No krummholz	Growth	Tissue formation (limited by a lack of heat)
		Into krummholz	Growth and dieback	Tissue formation + winter desiccation, snow moulds, browsing, abrasion

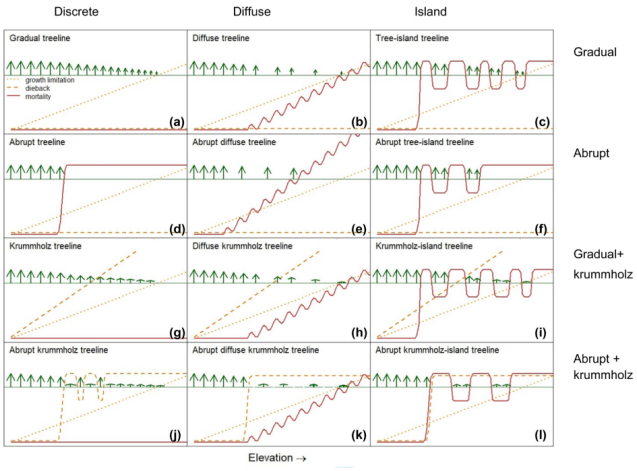

Figure 2: Left: Matrix of 2D spatial pattern, stature change and ecological processes which can contribute to the different types of ATEs. Source: @baderGlobalFrameworkLinking2021, Table 1. Right: Matrix of the multidimensional state space of treeline forms depicting extreme cases of the different dimensions. Columns represent the spatial patterns in the x-y plane and rows the change in tree stature (size and shape). The lines represents the hypothesized first-level ecological processes behind the patterns along an elevational gradient. The dotted line displays the growth limitation, the dashed line the dieback and the continuous line the mortality. Growth limitation always occurs while dieback only affects if krummholz is involved. Source: @baderGlobalFrameworkLinking2021, Figure 3.

To better understand and categorize ATEs a standardized description and terminology of spatial patterns has been proposed on hillslope and landscape scale by Bader et al. (2021), including hypotheses for the general mechanisms behind the patterns. The terminology and the multidimensional state-space can be most clearly understood from Figure 4.

After the definition and the characterization of the spatial patterns of ATEs, the following overview of ATE research shall serve as a basis for the workflow proposed in this methodological paper to globally detect ATEs.

2 Overview of Alpine Treeline Ecotone Research with focus on methodology

As already implied, Alpine Treeline Ecotone analysis has been carried out so far at local, regional and global scales with different focus. Chhetri & Thai (2019) investigate the use of GIS and remote sensing methods in ATE research between 1980 and 2017 and demonstrate that with the advances in sensor technology the access to higher resolution data and different data types the analysis methods diversify. Often it is hard to distinguish between the different methodological approaches because they all rely and depend on one-another and studies have usually applied multiple methods and methods have been applied for diverse scopes. The following overview of methods is crude and by no means comprehensive.

2.1 Statistical – analytical approach

Until the dispersal of openly available remote sensing products the approach was mainly concentrated on physiological/response based investigations with statistical analysis of local indicators based on in situ measurements. The main question was mainly: which environmental drivers control the location of ATE's and how complex are these (Körner 1998)? Drivers were differentiated on global, regional and local levels (Holtmeier – Broll 2005). As the main global driver temperature was defined (Körner (1998), Koerner (2012), Holtmeier & Broll (2007), 2, Bonanomi et al. (2018)), but at regional and local levels it looks more diverse: topography (Brown (1994), Virtanen et al. (2004) and Bader & Ruijten (2008)), geomorphologic processes, herbivory or anthropogenic disturbance (Chhetri & Thai (2019)). Analysis of topographic actors with logistic regression was used frequently (e.g Brown (1994), Virtanen et al. (2004) and Bader & Ruijten (2008)).

2.2 Remote sensing approach

The detection or localization of ATEs is facilitated by the availability of remote sensing data (satellite, airborne lately hyperspectral and UAV derived ortho/imagery). Specialized sensors operating in the R, G, B, IR, short-wave, hyperspectral and thermal regions of the electromagnetic spectrum give the possibility to approach and work with the specific spectral signatures (due to different absorption and reflection of radiation) of different vegetation entities. LiDAR

data enables to include the factor height thus moving the analysis of treelines in a 3D space. The main focus of this methodological paper is on the remote sensing approach (automated detection) and exemplary papers are accentuated in a short summary. The use of GIS and remote sensing has been constantly increasing in treeline studies since 2000, with a few preceding pioneers. Earlier studies concentrated on mapping treeline positions and lately the interest shifted towards factors that control treeline variation (Chhetri & Thai (2019), 1543). It can also be seen that with the development of the respective sensors the interest and use moved to data with higher spatial resolution (LiDAR data, Hyperspectral data), which on the other hand attracts more cost and thus often thins out the studies due to the lack of monetary resources and also the use of proprietary software, which shows that there is a lot to do in means of open-source and reproducible best-practice applications and code. Usually there is little information on the software used. The use of remotely sensed data is usually combined with classical approaches like statistical analysis in complex research questions, from which the following main directions emerge:

2.2.1 *Mapping of ATEs*

To map ATEs, studies use aerial photographs and Landsat imagery to identify and quantify treelines (Brown (1994), W. L. Baker et al. (1995), Allen & Walsh (1996), Kimball & Weihrauch (2000), Virtanen et al. (2004), and Resler et al. (2004)) but often also vegetation indices are used Myneni et al. (1997), Singh et al. (2015), and Mohapatra et al. (2019)) to analyse treeline elevation (Allen & Walsh (1996) and Kimball & Weihrauch (2000)) and topographic variables/geomorphological parameters (slope, angle, curvature, relief) to explain treeline structure (patch-metrics) (Kimball & Weihrauch (2000)). Tree population parameters are derived via PCA (e.g W. Baker & Weisberg (1997)) and also species distribution modelling is a usual application (Chhetri et al. (2017)).

2.2.2 *Montitoring ATEs/Change detection*

ATEs are space and time related phenomenons and they respond to changing environmental conditions, that is they can be sensitive to climate change (Singh et al. (2015), Holtmeier & Broll (2005), Holtmeier & Broll (2007), Harsch & Bader (2011), and Bader et al. (2021)). The rise in global average temperatures seems to lead to the geographically varying shifting

of ecotones: on regional level to upward shift ((Mohapatra et al., 2019)) but also stable or retracting ATEs can be determined (Winings (2013)). It still has to be understood if the results are due data quality. The identification and quantification of change in the ATEs can be carried out with regional and global monitoring of ATEs (Chhetri & Thai (2019)).

2.2.3 *Automated detection and mapping of ATEs*

Recently several research projects, Master theses and PhDs have investigated (semi-)automated detection and mapping methods of ATEs (see a list until 2013 in Winings (2013) and the also the recent literature). The availability of high resolution data facilitate the use of more and more sophisticated methods. In this methodological paper we are concentrating specifically on automated analysis.

Automated methods imply the use of specific algorithms to extract information from remote sensing data, either Pixel- or Object Based or recently also via Deep Learning (mainly CNNs). Some studies compare Object- and Pixel-based or different Object-based segmentation methods (Immitzer et al. (2012), Winings (2013), and Kupková et al. (2017)). Further it has to be emphasized, that the automated detection of ATEs relies heavily on tree detection. Parallel to elaborated workflows for the automated detection of ATEs improvements are made continuously on tree detection methods and tree cover estimation (Whiteside et al. (2020)) closely connected to the development of sensors and new data processing methods (Qiu et al. (2020), Weinstein et al. (2019) and Weinstein et al. (2020)) and form an important basis for automated analysis. In the following the most prominent automated methods are presented shortly including a few case studies.

Pixel-based Image Analysis is working with the information encoded in pixels – it assigns each pixel to a specific class on the basis of the respective values of the spectral bands or index or morphometric information (slope, aspect, etc.). One drawback is, that the context of the pixels and it's neighborhood gets neglected and the pixel values can be affected by circumstantial effects, like reflectance differences (Stueve et al. (2011)), shadow or clouds (Allen & Walsh (1996)). Also it doesn't deal, with textures per se, and for this a textural analysis has to be done by using different filters (mean, sobel, focal, etc.).

Resler et al. (2004) use panchromatic aerial imagery where they incorporate spectral (brightness values) and spatial (textural) information to classify 4 classes (tundra/bare, alpine meadow,

open forest/krummholz and closed canopy) representing the ATE using the maximum likelihood algorithm. A classification with and without textural information was done to assess the meaningfulness of textural information. The ERDAS modeler was used to extract textures.

Král (2009) uses CIR orthophotos to do a "classical" landcover classification using the maximum likelihood classifier, which then is reclassified into 2 classes (spruce canopies and other). Subsequently a focal filter is applied to the spruce canopy closure class for texture analysis, which is then reclassified into 5 classes (no trees, emergent trees, groups of trees, open-canopy forest, closed canopy forest). Class 3, that is groups of trees (26-50% spruce), neighbouring to alpine grassland and open-canopy forest was defined as ATE.

Immitzer et al. (2012) used WW-2 satellite data (8 + 4 bands) for the identification of 10 tree species by means of Random forest classification (object-based vs. pixel-based) using spectra of a) manually delineated tree crowns b) derived tree crown polygons and reference samples for tree species.

Winings (2013) used high resolution aerial imagery and LiDAR data in her Master's thesis to map the alpine treeline. She compared pixel- and object based classification. She used four different data input for both classification methods: NDVI, NDVI + multispectral aerial imagery, NDVI + tree height or NDVI + multispectral aerial imagery + tree height. In the case of the pixel-based classification the maximum likelihood and the unsupervised ISODATA (Iterative Self-Organizing Data Analysis Technique) clustering algorithms were compared. For the object-based image analysis multi-resolution segmentation was conducted, using colour and shape homogeneity. After the segmentation, the classes (tree vs. non-tree) were assigned based on object feature threshold. The accuracy for the pixel-based classifications was between 85.3 and 88.4 and for the object-based classification between 81.5 and 92.9 %, resulting in the best classification on the dataset with NDVI + multispectral aerial imagery + tree height. For the pixel-based image analysis ENVI and ERDAS and for the object-based analysis eCognition was used.

Kupková et al. (2017) used airborne hypersepctral (APEX and AISA DUAL) and Sentinel-A data for the classification of tundra vegetation by comparing pixel-based and object-based image analysis. Reference data was collected corresponding to 8 vegetation classes (anthropogenic areas, picea abies, pinus mugo dense, pinus mugo sparse, closed alpine grassland, grasses, alpine

heathlands, wetlands and peat bogs; with a detailed and a simplified legend). Based on the difference in resolution the hyperspectral data and the Sattelite imagery was classified separately. Latter was only classified pixel-based and with SVM (Support Vector Machines with radial basis function), NN (Neural Net) and MLC (Maximum Likelihood Classification) algorithms. The hyperspectral data, having a higher spatial resolution was classified pixel- and object-based. For the pixel-based classification the SVM, NN and MLC algoriths were used. For the objcet-based classification Edge-based segmentation was used on the hyperspectral datasets. The hyperspectral data yielded better classification result thean the Satellite data, with SVM pixel-based classification. ENVI was used for the study.

Object-based Image Analysis (GeOBIA) on the other hand is dealing with the grouping of pixels in homogeneous groups, that is segments which bear similar spectral, spatial and textural information. From each segment additional information can be extracted (statistical information, size, shape and context). Different segmentation algorithms exist, which treat the image and the segments different.

Middleton et al. (2008) used the Feature Extraction Module (Fx) implemented in ENVI to extract tree crowns from two aerial photographs (one from 1947 and one from 2003) via segmentation and feature classification with SVMwith textural, spatial and spectral information. The results were compared to forest inventory information and an upward shift was recorded on Lommoltunturi fell.

Ranson et al. (2011) used MODIS VCF (Vegetation Continuous Fields) tree cover data and segmentation to delineate the circumpolar taiga-tundra ecotone (TTE). The multi-annual VCF was adjusted usingf linear regressions and a vector layer was applied with previously delineated taiga and tundra biomes. Also the water bodies were masked out. Subsequently multi-resolution segmentation was carried out with eCongnition based on the homogeneity criterion. The resulting polygons were then classified on a specific range of adjusted VCF values which represent the TTE.

Mishra et al. (2018) used a UAV equipped with a Parrot Sequoia multispectral (Red, Green, Blue, Red Edge, Near Infra-Red) camera to acquire high resolution Imagery. Subsequently an SfM Orthoimage was calculated and then multi-resolution (based on the homogeneity criterium of scale, shape/colour and compactness/smoothness) and spectral difference segmenta-

tion (merging neighbouring objects based on a spectral threshold) was combined in eCognition to generate optimal feature space variables for the classes. Then the Random Forest Classifier was used for classification with 3 sets of features (spectral features; spectral features + geometric/shape features; spectral features + geometric/shape features + textural features) for species-level mapping of vegetation in the Himalayas.

Whiteside et al. (2020) used derivatives of aerial imagery and WW2 satellite data (TGI, NDVI) resampled to 1 m filtered by a low-pass filter. Then a threshold-based multi-resolution segmentation was conducted with eCognition to assess the tree cover (in percentage) for each date (1964, 1976, 1981, 2010). The results were compared by date to assess the tree cover reduction (4%) during the 36 years.

Geping Luo & Li Dai (2013) used aerial imagery from 1962 and 1981, QuickBird Satellite image from 2006 was used as data input to map vegetation distribution after orthorectification, and generating a DEM. The land-cover types were delineated: Schrenkiana, Sabina and other. Multi-resolution (?) segmentation was conducted in eCognition subsequently combined with a k-nearest neighbour classification. The result was compared with fieldwork data collection (2010, 2011) of the two species. With the post-classification approach the land-cover change was examined between 1962, 1981 and 2006.

Qiu et al. (2020) proposed a new spectral multi-scale (SMS) individual tree crown (ITC) delineation method using both brightness and spectra of high-resolution multrispectral imagery to be able to better delineate tree crowns in deciduous or mixed forests, where adjacent tree crowns are very close to each other. As the first step a morphological gradient map is calculated of multispectral images, then as a second step an inverse gradient image. Then initial treetops were extracted by multi-scale filtering and morphological operations with regard to tree crown shape which then were refined with the spectral reference of the neighbouring treecrowns (tree trops map). Subsequently the morphological gradient map is segmented by marker-controlled watershed segmentation which is then refined by the tree tops map, to receive an individual tree crown delineation map.

Deep Learning – contrary to pixel-based and GeOBIA – works on scene level and enables thus to deal better with the complex semantic structure of the increasing resolution of remote sensing images. A multitude of different Deep Learning models exist with different structures

to fulfill different aims (e. g. segmentation, classification). The most common Deep Learning model structure are CNNs – Convolutzional Neural Networks, which are multi-layer networks with learning ability that consists of convolutional layers, pooling layers, and fully connected layers.

Fricker et al. (2019) used airborne hyper-spectral imagery, LiDAR data and a CNN (Convolutional Neural Network) to automate tree species classification. 7 dominant tree species and a dead tree class were identified to serve as reference data for the CNN. A LiDAR derived CHM was used to digitize the individual tree canopies to prepare their pixels for the species labelling for the CNN. The classification was executed separately on the RGB and the hyper-spectral data. The classification with the hyper-spectral data (0.73 – 0.90) yielded better classification results than the RGB classification (0.41 – 0.88). All code and data to ensure reproducibility can be found online.

Weinstein et al. (2019) proposed a semi-supervised CNN workflow based on the comparision of 3 unsupervised tree-crown segmentation algorithms. The result of the chosen tree crown segmentation (clustering of a CHM by tree height and crown width) of the LiDAR data was extracted as a bounding box from the RGB image, which' data set is then labeled self-supervised and pretrained by a retinanet CNN. Then the CNN was retrained with a small hand-annotated dataset (supervised classification), to correct errors from the initial un-supervised segmentation, which indeed improved the results of the prediction.

Weinstein et al. (2020) build on the results from **Weinstein et al. (2019)** 2019 and tested if training datasets can be generalized and be used on completely different forested areas. Generally the performance of the model performance decreased, but when they were applied to spatially and spectrally similar forested areas the performance increased. Best was again, when the CNN was retrained by a handful of hand-annotated data from the same area.

Based on this literature review and the available data sets it was decided to develop two separate workflows for Pixel Based Image Classification (using Satellite data) and Object Based Image Analysis (using LiDAR data) to combine the two workflows

3 Methodology

3.1 Description of the research area and the data sets used in the case study

The workflow is presented on a case study area in the Vorarlberg, Alps…

Figure 3

3.2 The reproducible workflow

The reproducible workflow is made up of the files: **00_library_n_prep.R**, **0_set_up_working_envrnmt.R**, **1_data_prep_general.R**, **2_segmentation_test_area_1.R**, **3_segmentation_validation_ROI.R**, **4_data_prep_classification_test_area_1.R**, **5_classification_validation_test_area_1.R** and **6_data_prep_classification_ROI.R**, **7_classification_ROI.R**.

These commented R files build up on each other step-by-step, starting with the preprocessing of the input data. This .Rmd only presents the backbone which links the .R files together.

To reproduce the results of the whole project you have to run the code in the .R files, numbered sequentially. **00_library_n_prep.R** is a library file, containing all the packages needed for this project. It installs packages from the R repository or from github if some would be missing. This file does not need running, unlike the next one, **0_set_up_working_envrnmnt.R**. It is going to set up the project folder structure on your computer/laptop, but you have to adapt the path of the project directory to the destined place on your computer/laptop and also attach or install the packages needed. The data used in this project is stored on Google Drive, from where you have to download it to the respective folders (**dsm/**, **dem/**, **RGB_IR/**, **RGB_IR/**, **treepos/**, **train/**) set up on you device by the script you just ran (because a)**github** limits the size of data to be uploaded and b) the data used is not openly available, that is proprietary).

The main workflow consist of to sub-workflows, which are equally important: the Object Based Image Analysis (**.R files 2-3**, working with the LiDAR data set) and the Pixel-Based Image Classification (**.R files 4-5-6-7**, working with the Satellite data set), which will be combined at the end (**.R file 8**).

Flowchart of the workflow (Figure 4)

The .R files are commented in a manner, that they can be used as a manual or tutorial. In this chapter only the ideas behind the workflow and in the next chapter the results will be discussed to keep it short.

For this project three R packages were developed: *LEGION*, *CENITH* and *IKARUS*. **LEGION** computes indices from RGB and Multispectral Imagery and provides also their basic statistics (correlation and homogeneity). See more details in the help pages and in the tutorial of the package. **CENITH** is a wrapper for the *ForestTools package* (Plowright and Roussel 2020) to perform tree segmentation on a specific area. It also provides cross validation to estimate and validate the performance of a segmentation model for multiple test areas. See more details in the help pages and in the tutorial of the package.
IKARUS is a wrapper for the *CAST* package (Meyer 2020) to perform Pixel-based Image Analysis and classification.See more details in the help pages and in the tutorial of the package.

3.3 General data preparation (.R file: 1_data_prep_general.R)

For the project a Region of Interest (later ROI) was chosen which displays the different vegetation types at this specific ATE. Four test areas were defined within the ROI. The workflow is designed in such a way, that the individual steps of the workflow were developed on test area 1 and tested (generalized) on the other (test) areas to deal with the unavoidable variability of data. The resulting settings and variables are then to applied to the ROI. This three-step procedure is used to make sure that the algorithms applied and values used are effective and robust.

Originally masks for each 4 test areas were created in QGIS and based on them, the Canopy Height Model (CHM) and the RGB and IR (Infra-Red) imagery was cropped to the size of the test area masks. When it became clear, that the minimal computable raster size (on grounds of the restrictions of the 'raster' package in R) was a lot smaller than the maximum size of the actual ROI originally decided, it was reduced. The sizes of the CHM test areas were defined using the **'Clip raster by Extent'** tool, with the ***'use map canvas'*** setting in QGIS, to define 4, approximately 32 x 32 m test areas. Then the respective CHM test areas were used as masks/extents to clip the respective RGB and IR test areas in QGIS.

The CHM was created by subtracting the Digital Elevation Model (DEM) form the Digital Surface Model (DSM). This way only the LiDAR points connected to the vegetation above ground are preserved and can be used for our calculations.

3.4 Segmentation of the test area 1

(.R file: 2_segmentation_test_area_1.R)

The aim of this step is to find an accurate segmentation for test area 1 which can be tested on the other test areas and then applied to the ROI.

The segmentation is performed using the CENITH package. As CENITH is a wrapper for ForestTools, it also uses the **Watershed Segmentation** using markers (Meyer and Beucher 1990) which is implemented in ForestTools.

The first task is to set verification points (this can be also done with the ForestTools package, but we preferred to do it by hand so it was not implemented in the CENITH package) - that is locate the positions of the trees (we will call it tree positions but technically they are verification points, that is 'vp') in the test areas using QGIS.

Before starting to define the tree positions in each test areas, first of all the minimum height of the trees has to be identified (which of course is region and area dependent). In the Alpine region the vegetation consists of trees but also shrubs and Krummholz, which have to be distinguished from trees. If also young trees trees are present and should be considered, then it is important not to confuse them with shrubs, which is often rather complicated and even impossible. If Satellite Imagery is also available (as in our case), it can help to consider the difference in the spectral and textural signature. The identification of the minimum tree-height can be best determined using QGIS. Thus to distinguish the actual trees, for one the spectral information of the Satellite Imagery (which will be mainly used for the Pixel-based Image Classification) was exploited. Trees demonstrate - apart from their height in the CMHs - much more branches which leads to less homogeneous green color (mixed with black and creme colored pixels) as that of the shrubs which show in their entirety a single color. On the other side the CHMs were displayed by giving each height between < 0.5 m and > 29 ma different color (see the QGIS style file). Combining these two sets of information, the minimum tree height was defined at 4-5 meters (Figure 5). This height included the lowest young trees but not the shrubs and

Krummholz. To be able to include the young trees, it was opted for h=4 instead of 5 meters.

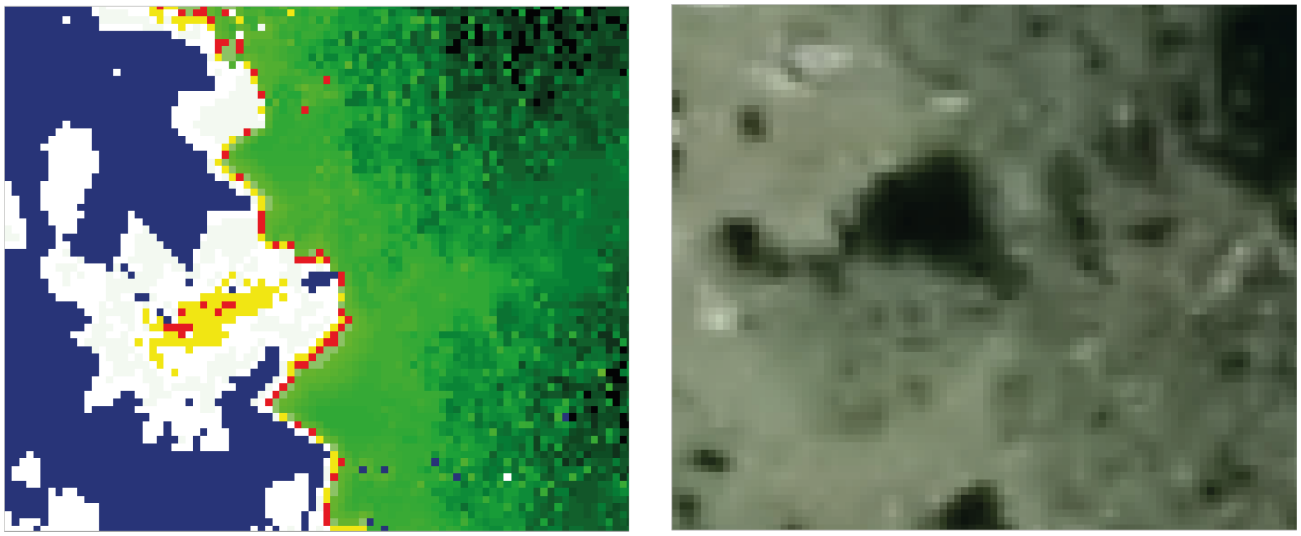

Figure 3: Comparision of RGB Satellite Imagery and LIDAR-derived CHMs classified by height using different colors (blue < o.5 m; white > 0.5 < 3; yellow > 3 < 4m, red > 4 < 5m; green to black < 5m) Detail of test area 4.

The exact position of the individual trees (including young trees) was based for on on the decision of the minimum tree height based on the RGB and IR Satellite Imagery and was determined by looking for the highest point of the chms.

```
## Reading layer `vp_1' from data source
##   `C:\Users\kelto\Documents\detectATE\analysis\data\treepos\vp_1.shp'
##   using driver `ESRI Shapefile'
## Simple feature collection with 15 features and 1 field
## Geometry type: POINT
## Dimension:     XY
## Bounding box:  xmin: -40638.55 ymin: 216053.3 xmax: -40615.55 ymax: 216083.1
## Projected CRS: MGI_Austria_GK_West_with_axis_order_normalized_for_visualization
```

The segmentation itself can be executed with the **CENITH::TreeSeg** function. This function works with a MovingWindow of size a * b (x,y) at height h. *a*, *b* are horizontal and vertical values (x, y) in meters and *h* is height in meters on the CHM. This function takes single values, with which different and various values of the segmentation variable can be tested. The results can be checked in QGIS. The variables *MIN* and *MAX* filter the segments to a certain size. Because with the variables used there is small chance to get too big segments, the *MAX* variable

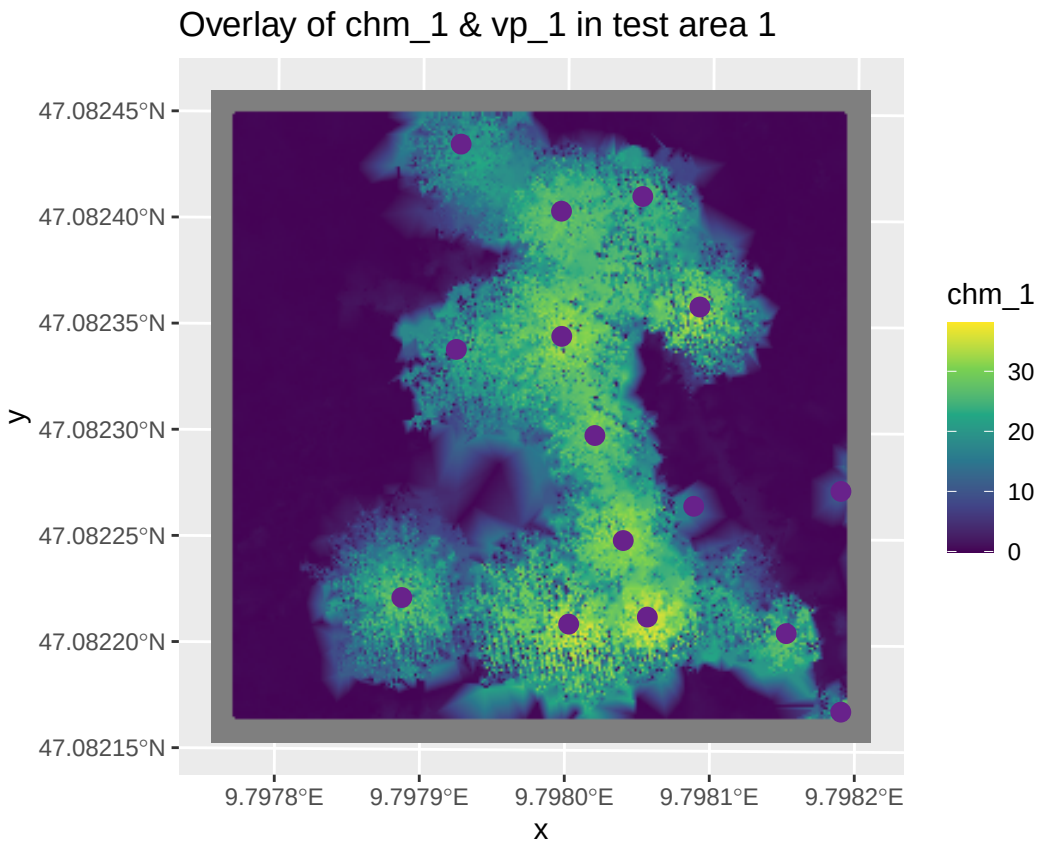

Figure 4: The defined tree positiions (verification points/vp) in IR Satellite Imagery of test area 1 .

is not used, only the *MIN* variable, to filter out small segments. Another variable, which controls and filters out small artifacts and data errors - directly on the chm is the *chmFilter*. The tests with **CENITH::TreeSeg** show, that it is very useful to apply a *sum* filtered CHM (see the difference between the results **test_0** and **test_1** in QGIS) and give an estimate of how big or small the variables *a*, *b* and *MIN* have to be set. Based on the fact that there are 15 trees in test area 1 we can estimate how accurate the segments might be. Taking a look at test 1, 2 & 3 we can see how the reduction of *a* and *b* elevated the number of trees. This is useful information for **CENITH::BestSegVal**.

The function **CENITH::BestSegVal** can be fed with long sequences of values for each variable (this is called parameter tuning). N.B. long sequences mean longer calculation time, thus it is best to test out different variable settings with **CENITH::TreeSeg** to narrow down in which setting range a, b and h might move. In the second part of the script *2_segmentation_test_area_1.R*, the use of **CENITH::BestSegVal** is demonstrated. In this function also the vps (tree positions) are taken into account as a validation basis. All calculation in the resulting table are based on the comparison of the vps/tree positions to the segmentation results. The variable *hit.vp* shows explicitly, how many vps/tree positions are 'hit' by the resulting segments.

In the first run the values **a=seq(0.05, 0.1, 0.01), b=seq(0.05, 0.1, 0.01), h=seq(3.5, 6, 0.5), MIN=seq(0.1, 0.5, 0.1)** were tested, to go a bit below and above the defined height of the trees and to determine the best *a*, *b* and *MIN* values. *CHMfilter* is set at 3, because we want to do only minimal filtering to minimize small artifacts and gaps in the chm. In the first run we got 1080 results and 45 maximal segments. Because there are 15 trees in test area 1, the tibble was filtered to 20 segments (to count in possible undersegmentation) and arranged according to the best *hitrate* (which was 0.733333) and still got 664 results. These are still too much results to decide which combination of settings should be applied to the other test areas. Thus the results were filtered to a **hitrate >= 0.7** (the best results), **height <= 4.0.** (the height of trees) and the total segments were ordered in descending order. This resulted in 40 observations, from which the first four were actually calculated with *TreeSeg* and compared in QGIS. The lesson learend was, that it became clear that MIN (the size of the smallest segment) has to be set to 0.1 and that the range of a & b of the best results is > 0.1.

Thus a second run of **CENITH::BestSegVal** was set up with the variables **MIN=0.1,**

a=seq(0.01, 0.1, 0.01), b=seq(0.01, 0.1, 0.01), to find better segment sizes and **h=seq(3.5, 6, 0.5)** with the same settings as in the first run, to enable a systematic analysis. The 600 results were filtered the same way as the first run: filtering to 20 segments lead to 204 results, still keeping the best *hitrate* at 0.733333. The filtering to **hitrate >= 0.7** and **height <= 4.0** lead to 8 observations, of which six are the same results of the first round. These correspondence of these 8 results confirmed, that all should be applied to the other test areas in the next step (*3_segmentation_validation_area_1_ROI.R*). All steps can be computed in the respective .R files.

Table 1: Results of the second run of CENITH::BestSegVal

a	b	height	total_seg	hit.vp	under	over	area	hitrate	underrate	overrate	Seg_qualy	MIN	chm
0.07	0.07	3.5	20	11 / 15	2	7	543.1406	0.7333333	0.1000000	0.3500000	0.73 @ 0.28	0.1	chm_1_3
0.07	0.08	3.5	20	11 / 15	2	7	543.1406	0.7333333	0.1000000	0.3500000	0.73 @ 0.28	0.1	chm_1_3
0.07	0.09	3.5	20	11 / 15	2	7	543.1406	0.7333333	0.1000000	0.3500000	0.73 @ 0.28	0.1	chm_1_3
0.07	0.07	4.0	20	11 / 15	2	7	535.0156	0.7333333	0.1000000	0.3500000	0.73 @ 0.28	0.1	chm_1_3
0.07	0.08	4.0	20	11 / 15	2	7	535.0156	0.7333333	0.1000000	0.3500000	0.73 @ 0.28	0.1	chm_1_3
0.07	0.09	4.0	20	11 / 15	2	7	535.0156	0.7333333	0.1000000	0.3500000	0.73 @ 0.28	0.1	chm_1_3
0.07	0.10	3.5	19	11 / 15	2	6	543.1562	0.7333333	0.1052632	0.3157895	0.73 @ 0.26	0.1	chm_1_3
0.07	0.10	4.0	19	11 / 15	2	6	535.0156	0.7333333	0.1052632	0.3157895	0.73 @ 0.26	0.1	chm_1_3

3.5 Cross-validated Segmentation of test areas

(.R file: 3_segmentation_validation_area_1_ROI.R)

The filtered results of the segmentation of test area 1 resulted in eight possible segmentations which are going to be tested if and how they fit the other test areas. Up to some degree it is an experiment to test which might be the possibly best segmentation which fits the other test areas. That is why all eight results from **best_seg_vp_1_filt_v2_filt** were processed. The eight results contain also h=3.5 m, so it can be checked which height really represents best the whole ROI. The cross-validates segmentation is done by the **CENITH::TreeSegCV** function. The test areas and vps (tree positions) are given as a list to the function. The length of both lists/number of test areas and vps have to equal. The number of test areas and vps set the number of folds used, in this case 4. It gives a similar table as result as **CENITH::BestSegVal**, but calculates also the overall performance of the segmentation quality (which is based on how many and how much of the vps/tree positions were 'hit'), printed out when the cross-validated segmentation has finished. All eight settings produce on

Table 2: Results of the cross-validations cv1 - cv8

cv1	sites	a	b	height	total_seg	hit	vp	under	over	area	hitrate	underrate	overrate	Seg_qualy
1	chm_1	0.07	0.07	4	20.0	11.00	15.00	2.0	7.00	535.0156	0.7333333	0.1000000	0.3500000	0.73 @ 0.28
2	chm_2	0.07	0.07	4	28.0	10.00	12.00	1.0	17.00	421.0312	0.8333333	0.0357143	0.6071429	0.83 @ 0.34
3	chm_3	0.07	0.07	4	40.0	16.00	18.00	1.0	23.00	605.9531	0.8888889	0.0250000	0.5750000	0.89 @ 0.31
4	chm_4	0.07	0.07	4	22.0	8.00	12.00	2.0	12.00	369.2031	0.6666667	0.0909091	0.5454545	0.67 @ 0.36
5	Mean	0.07	0.07	4	27.5	11.25	14.25	1.5	14.75	482.8008	0.7805556	0.0629058	0.5193994	0.78 @ 0.32

cv2	sites	a	b	height	total_seg	hit	vp	under	over	area	hitrate	underrate	overrate	Seg_qualy
1	chm_1	0.07	0.08	3.5	20.00	11.00	15.00	2.0	7.0	543.1406	0.7333333	0.1000000	0.3500000	0.73 @ 0.28
2	chm_2	0.07	0.08	3.5	28.00	10.00	12.00	1.0	17.0	443.3438	0.8333333	0.0357143	0.6071429	0.83 @ 0.34
3	chm_3	0.07	0.08	3.5	43.00	16.00	18.00	1.0	26.0	623.5000	0.8888889	0.0232558	0.6046512	0.89 @ 0.33
4	chm_4	0.07	0.08	3.5	22.00	8.00	12.00	2.0	12.0	377.0000	0.6666667	0.0909091	0.5454545	0.67 @ 0.36
5	Mean	0.07	0.08	3.5	28.25	11.25	14.25	1.5	15.5	496.7461	0.7805556	0.0624698	0.5268121	0.78 @ 0.33

cv3	sites	a	b	height	total_seg	hit	vp	under	over	area	hitrate	underrate	overrate	Seg_qualy
1	chm_1	0.07	0.09	3.5	20.0	11.00	15.00	2.0	7.00	543.1406	0.7333333	0.1000000	0.3500000	0.73 @ 0.28
2	chm_2	0.07	0.09	3.5	27.0	10.00	12.00	1.0	16.00	443.4219	0.8333333	0.0370370	0.5925926	0.83 @ 0.33
3	chm_3	0.07	0.09	3.5	42.0	16.00	18.00	1.0	25.00	623.5156	0.8888889	0.0238095	0.5952381	0.89 @ 0.32
4	chm_4	0.07	0.09	3.5	21.0	8.00	12.00	2.0	11.00	377.0156	0.6666667	0.0952381	0.5238095	0.67 @ 0.36
5	Mean	0.07	0.09	3.5	27.5	11.25	14.25	1.5	14.75	496.7734	0.7805556	0.0640212	0.5154101	0.78 @ 0.32

cv4	sites	a	b	height	total_seg	hit	vp	under	over	area	hitrate	underrate	overrate	Seg_qualy
1	chm_1	0.07	0.07	3.5	20.00	11.00	15.00	2.0	7.0	543.1406	0.7333333	0.1000000	0.3500000	0.73 @ 0.28
2	chm_2	0.07	0.07	3.5	28.00	10.00	12.00	1.0	17.0	443.3438	0.8333333	0.0357143	0.6071429	0.83 @ 0.34
3	chm_3	0.07	0.07	3.5	43.00	16.00	18.00	1.0	26.0	623.5000	0.8888889	0.0232558	0.6046512	0.89 @ 0.33
4	chm_4	0.07	0.07	3.5	22.00	8.00	12.00	2.0	12.0	377.0000	0.6666667	0.0909091	0.5454545	0.67 @ 0.36
5	Mean	0.07	0.07	3.5	28.25	11.25	14.25	1.5	15.5	496.7461	0.7805556	0.0624698	0.5268121	0.78 @ 0.33

cv5	sites	a	b	height	total_seg	hit	vp	under	over	area	hitrate	underrate	overrate	Seg_qualy
1	chm_1	0.07	0.08	4	20.0	11.00	15.00	2.0	7.00	535.0156	0.7333333	0.1000000	0.3500000	0.73 @ 0.28
2	chm_2	0.07	0.08	4	28.0	10.00	12.00	1.0	17.00	421.0312	0.8333333	0.0357143	0.6071429	0.83 @ 0.34
3	chm_3	0.07	0.08	4	40.0	16.00	18.00	1.0	23.00	605.9531	0.8888889	0.0250000	0.5750000	0.89 @ 0.31
4	chm_4	0.07	0.08	4	22.0	8.00	12.00	2.0	12.00	369.2031	0.6666667	0.0909091	0.5454545	0.67 @ 0.36
5	Mean	0.07	0.08	4	27.5	11.25	14.25	1.5	14.75	482.8008	0.7805556	0.0629058	0.5193994	0.78 @ 0.32

cv6	sites	a	b	height	total_seg	hit	vp	under	over	area	hitrate	underrate	overrate	Seg_qualy
1	chm_1	0.07	0.09	4	20.00	11.00	15.00	2.0	7	535.0156	0.7333333	0.1000000	0.3500000	0.73 @ 0.28
2	chm_2	0.07	0.09	4	27.00	10.00	12.00	1.0	16	421.1094	0.8333333	0.0370370	0.5925926	0.83 @ 0.33
3	chm_3	0.07	0.09	4	39.00	16.00	18.00	1.0	22	605.9531	0.8888889	0.0256410	0.5641026	0.89 @ 0.31
4	chm_4	0.07	0.09	4	21.00	8.00	12.00	2.0	11	369.2344	0.6666667	0.0952381	0.5238095	0.67 @ 0.36
5	Mean	0.07	0.09	4	26.75	11.25	14.25	1.5	14	482.8281	0.7805556	0.0644790	0.5076262	0.78 @ 0.32

cv7	sites	a	b	height	total_seg	hit	vp	under	over	area	hitrate	underrate	overrate	Seg_qualy
1	chm_1	0.07	0.1	3.5	19.0	11.00	15.00	2.0	6.00	543.1562	0.7333333	0.1052632	0.3157895	0.73 @ 0.26
2	chm_2	0.07	0.1	3.5	26.0	10.00	12.00	1.0	15.00	443.4688	0.8333333	0.0384615	0.5769231	0.83 @ 0.33
3	chm_3	0.07	0.1	3.5	41.0	16.00	18.00	1.0	24.00	623.5781	0.8888889	0.0243902	0.5853659	0.89 @ 0.32
4	chm_4	0.07	0.1	3.5	20.0	8.00	12.00	2.0	10.00	377.0312	0.6666667	0.1000000	0.5000000	0.67 @ 0.35
5	Mean	0.07	0.1	3.5	26.5	11.25	14.25	1.5	13.75	496.8086	0.7805556	0.0670287	0.4945196	0.78 @ 0.31

cv8	sites	a	b	height	total_seg	hit	vp	under	over	area	hitrate	underrate	overrate	Seg_qualy
1	chm_1	0.07	0.1	4	19.00	11.00	15.00	2.0	6	535.0156	0.7333333	0.1052632	0.3157895	0.73 @ 0.26
2	chm_2	0.07	0.1	4	26.00	10.00	12.00	1.0	15	421.1406	0.8333333	0.0384615	0.5769231	0.83 @ 0.33
3	chm_3	0.07	0.1	4	38.00	16.00	18.00	1.0	21	605.9531	0.8888889	0.0263158	0.5526316	0.89 @ 0.3
4	chm_4	0.07	0.1	4	20.00	8.00	12.00	2.0	10	369.2500	0.6666667	0.1000000	0.5000000	0.67 @ 0.35
5	Mean	0.07	0.1	4	25.75	11.25	14.25	1.5	13	482.8398	0.7805556	0.0675101	0.4863360	0.78 @ 0.31

all test areas an overall performance (mean performance in Table 1) between 0.78 @ 0.31 and 0.78 @ 0.33. This value is given right away by the algorithm as result. Looking at the data frame created by each cross-validated segmentation, the following can be observed (Table 2):

Inspecting the performance of the individual test areas, it is visible, that the behave similarly in each segmentation, but also that test area 4 has the lowest values all variables considered. This shows, that the performance of the different test areas depend on each other and balance each other out.

3.6 Segmentation of ROI (4_segmentation_ROI.R)

Given the explanatory aim of this work, all eight results of **best_seg_vp_1_filt_v2_filt** (created in Chapter 3.4 and tested on all 4 test areas in Chapter 3.5) were applied to the ROI. The segmentation results can be visually inspected and compared in QGIS. It became swiftly clear (as expected), that h=3.5 m is too low as tree height because it may result in segmenting some of the shrub as well (note the different colors of the chm heights in QGIS). Because of the similar height of the seedlings and young trees and shrubs it is practically impossible to distinguish shrubs and seedlings based purely on height (as discussed before) and thus the choice of 4 m as tree height was not revised.

All segmentations demonstrate almost the same overall performance between 0.78 @ 0.31 and 0.78 @ 0.33. Comparing the segmentation results in QGIS visually, **segm_ROI_8** delivers the best result:

Table 3: Settings of **segm-ROI-8**

a	b	height	total_seg	hit.vp	under	over	area	hitrate	underrate	overrate	Seg_qualy	MIN	chm
0.07	0.1	4	19	11 / 15	2	6	535.0156	0.7333333	0.1052632	0.3157895	0.73 @ 0.26	0.1	chm_1_3

Although **segm_ROI_8** is not so accurate with the number and size/area of the individual trees, it is by far the most accurate segmentation which segments only trees and in some instances young trees.

But what happens with heights above 4 m? 4.5, 5 and 5.1 m (**segm_ROI_9** to **segm_ROI_12**) were tested to test if the results of **segm_ROI_8** can be refined. With a tree-height over 4 m, the number of charted young trees and the tree crown area is decreasing. Thus the optimal result is **segm_ROI_8**. You can see the results of the segmentations in the respective script. It has to be underlined, that the segmentation is of course not perfect - approximately 78%. It has to be said that it makes no real sense to thoroughly compare the segmentation results with the RGB Imagery - rather the IR Imagery; The segmentation is based on the Canopy Height Model and height data and the RGB and IR Imagery on spectral data. E.g. in the IR Imagery you can see the young trees and seedling in a lighter red.

```
## Reading layer `segm_ROI_8' from data source
```

```
##   `C:\Users\kelto\Documents\detectATE\analysis\results\segm\segm_ROI\segm_ROI_8.shp'
##   using driver `ESRI Shapefile'
## Simple feature collection with 786 features and 4 fields
## Geometry type: POLYGON
## Dimension:     XY
## Bounding box:  xmin: -40847 ymin: 215899.4 xmax: -40595.5 ymax: 216089.5
## CRS:           unknown
```

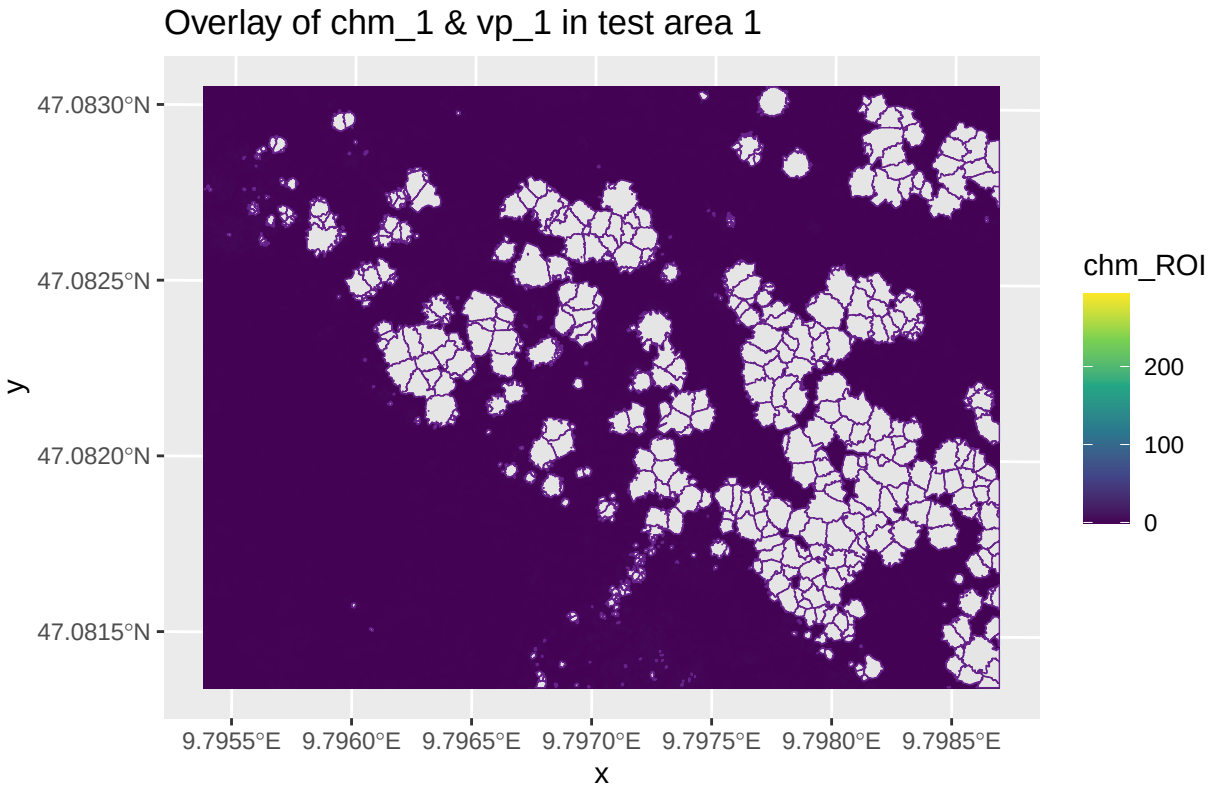

3.7 Data preparation for the Classification (.R file: 4_data_prep_classification:area_1.R)

For the preparation for the spectral classification first we will compute RGB and then multi-spectral (MS) indices, which will be filtered and then tested on correlation. Following that 10 predictor sets are built which will be tested in the next step (Chapter 3.8). Indices are used to enhance the spectral differences between the different object classes which are to be detected. Currently 11 RGB and 4 MS indices are implemented. Additionally the filter en-

hance special properties of indices and the overall homogeneity of spectral areas and enhance the edges and between the different objects. During the testing it was understood, that there are certain indices which contain too homogeneous areas from the beginning thus filtering them would distort the values and they would not be kicked out by the correlation and would deform the prediction. Thus three different index stacks were complied: *RGB_1_ind (VVI, VARI, NDTI, RI, CI, BI,SI,HI, TGI, GLI, NGRDI) RGB_1_ind2 (VVI, NDTI, CI, BI, SI, TGI, GLI, NGRDI)* Which were then stack together to form the following data stacks: *ALL_1_stack (RGB_1_ind, RGBNIR_1_ind)* 15 layer *ALL_1_stack2 (RGB_1_ind2, RGBNIR_1_ind)* 12 layer *ALL_1_stack3 (RGB_1_ind, RGBNIR_1_ind, RGBNIR_1)* had been corrected by subtracting HI: 18 layer Different data stacks were tested to see if more data would filter out/overlay the shortcomings of certain indices. The homogeneity test filtered out the homogeneous indices, that is also VARI and RI, but HI had to be extracted separately.

4 Results

5 References

Allen, T. R., & Walsh, S. J. (1996). Spatial and compositional pattern of alpine treeline, Glacier National Park, Montana. *Photogrammetric Engineering and Remote Sensing (USA)*. https://scholar.google.com/scholar_lookup?title=Spatial+and+compositional+pattern+of+alpine+treeline%2C+Glacier+National+Park%2C+Montana&author=Allen%2C+T.R.+%28University+of+Vermont%2C+Burlington%2C+VT.%29&publication_year=1996

Bader, M. Y., Llambí, L. D., Case, B. S., Buckley, H. L., Toivonen, J. M., Camarero, J. J., Cairns, D. M., Brown, C. D., Wiegand, T., & Resler, L. M. (2021). A global framework for linking alpine-treeline ecotone patterns to underlying processes. *Ecography*, *44*(2), 265–292. https://doi.org/10.1111/ecog.05285

Bader, M. Y., Rietkerk, M., & Bregt, A. K. (2007). Vegetation Structure and Temperature Regimes of Tropical Alpine Treelines. *Arctic, Antarctic, and Alpine Research*, *39*(3), 353–364. https://doi.org/10.1657/1523-0430(06-055)%5BBADER%5D2.0.CO;2

Bader, M. Y., & Ruijten, J. J. A. (2008). A topography-based model of forest cover at the alpine tree line in the tropical Andes. *Journal of Biogeography*, *35*(4), 711–723. https://doi.org/10.1111/j.1365-2699.2007.01818.x

Baker, W. L., Honaker, J. J., & Wiesberg, P. J. (1995). *Using aerial photography and GIS to map the forest-tundra ecotone in Rocky Mountain National Park, Colorado, for global change research.* https://scholar.google.com/citations?view_op=view_citation&hl=en&user=kgaHKiwAAAAJ&alert_preview_top_rm=2&citation_for_view=kgaHKiwAAAAJ:qjMakFHDy7sC

Baker, W., & Weisberg, P. (1997). Using GIS to model tree population parameters in the Rocky Mountain National Park forest–tundra ecotone. *Journal of Biogeography*, *24*(4), 513–526. https://doi.org/10.1111/j.1365-2699.1997.00130.x

Barredo Cano, J., Mauri, A., & Caudullo, G. (2020). *Impacts of climate change in European mountains: Alpine tundra habitat loss and treeline shifts under future global warming : JRC PESETA IV project : Task 8.* (No. JRC115186). Publications Office of the European Union. https://data.europa.eu/doi/10.2760/653658

Bonanomi, G., Rita, A., Allevato, E., Cesarano, G., Saulino, L., Di Pasquale, G., Allegrezza, M., Pesaresi, S., Borghetti, M., Rossi, S., & Saracino, A. (2018). Anthropogenic and environmental factors affect the tree line position of Fagus sylvatica along the Apennines (Italy). *Journal of Biogeography*, *45*(11), 2595–2608. https://doi.org/10.1111/jbi.13408

Brown, D. G. (1994). Predicting Vegetation Types at Treeline Using Topography and Biophysical Disturbance Variables. *Journal of Vegetation Science*, *5*(5), 641–656. https://doi.org/10.2307/3235880

Chhetri, P. K., Shrestha, K. B., & Cairns, D. M. (2017). Topography and human disturbances are major controlling factors in treeline pattern at Barun and Manang area in the Nepal Himalaya. *Journal of Mountain Science*, *14*(1), 119–127. https://doi.org/10.1007/s11629-016-4198-6

Chhetri, P. K., & Thai, E. (2019). Remote sensing and geographic information systems techniques in studies on treeline ecotone dynamics. *Journal of Forestry Research*, *30*(5), 1543–1553. https://doi.org/10.1007/s11676-019-00897-x

Elliott, G. P. (2017). Treeline Ecotones. In D. Richardson, A. Castree, M. F. Goodchild, A. Kobayashi, W. Liu, & R. A. Marston (Eds.), *The International Encyclopedia of Geography* (pp. 1–10.). Wiley & Sons. https://doi.org/10.1002/9781118786352.wbieg0539

Fricker, G. A., Ventura, J. D., Wolf, J. A., North, M. P., Davis, F. W., & Franklin, J. (2019). A Convolutional Neural Network Classifier Identifies Tree Species in Mixed-Conifer Forest from Hyperspectral Imagery. *Remote Sensing*, *11*(19), 2326. https://doi.org/10.3390/rs11192326

Geping Luo, & Li Dai. (2013). Detection of alpine tree line change with high spatial resolution remotely sensed data. *Journal of Applied Remote Sensing*, *7*(1), 1–14. https://doi.org/10.1117/1.JRS.7.073520

Harsch, M. A., & Bader, M. Y. (2011). Treeline form – a potential key to understanding treeline dynamics. *Global Ecology and Biogeography*, *20*(4), 582–596. https://doi.org/10.1111/j.1466-8238.2010.00622.x

Harsch, M. A., Hulme, P. E., McGlone, M. S., & Duncan, R. P. (2009). Are treelines advancing? A global meta-analysis of treeline response to climate warming. *Ecology Letters*, *12*(10), 1040–1049. https://doi.org/10.1111/j.1461-0248.2009.01355.x

Holtmeier, F.-K., & Broll, G. (2005). Sensitivity and response of northern hemisphere altitudinal and polar treelines to environmental change at landscape and local scales. *Global Ecology and Biogeography*, *14*(5), 395–410. https://doi.org/10.1111/j.1466-822X.2005.00168.x

Holtmeier, F. K., & Broll, G. E. (2007). Treeline advance - driving processes and adverse factors. *Landscape Online*, *1*, 1–33. https://doi.org/10.3097/LO.200701

Immitzer, M., Atzberger, C., & Koukal, T. (2012). Tree Species Classification with Random Forest Using Very High Spatial Resolution 8-Band WorldView-2 Satellite Data. *Remote Sensing*, *4*(9), 2661–2693. https://doi.org/10.3390/rs4092661

Kimball, K. D., & Weihrauch, D. M. (2000). Alpine vegetation communities and the alpine-treeline ecotone boundary in New England as biomonitors for climate change. *In: McCool, Stephen F.; Cole, David N.; Borrie, William T.; O'Loughlin, Jennifer, Comps. 2000. Wilderness Science in a Time of Change Conference—Volume 3: Wilderness as a Place for Scientific Inquiry; 1999 May 23–27; Missoula, MT. Proceedings RMRS-P-15-VOL-3. Ogden, UT: U.S. Department of Agriculture, Forest Service, Rocky Mountain Research Station. P. 93-101*, *015*. http://www.fs.usda.gov/treesearch/pubs/21974

Koerner, C. (2012). Was steuert das Pflanzenwachstum? *Biologie in Unserer Zeit*, *42*(4), 238–243. https://doi.org/10.1002/biuz.201210484

Körner, C. (1998). A re-assessment of high elevation treeline positions and their explanation. *Oecologia*, *115*(4), 445–459. https://doi.org/10.1007/s004420050540

Körner, C., & Paulsen, J. (2004). A world-wide study of high altitude treeline temperatures. *Journal of Biogeography*, *31*(5), 713–732. https://doi.org/10.1111/j.1365-2699.2003.01043.x

Král, K. (2009). Classification of Current Vegetation Cover and Alpine Treeline Ecotone in the Praděd Reserve (Czech Republic), Using Remote Sensing. *Mountain Research and Development*, *29*(2), 177–183. https://doi.org/10.1659/mrd.1077

Kupková, L., Červená, L., Suchá, R., Jakešová, L., Zagajewski, B., Březina, S., & Albrechtová, J. (2017). Classification of Tundra Vegetation in the Krkonoše Mts. National Park Using APEX, AISA Dual and Sentinel-2A Data. *European Journal of Remote Sensing*, *50*(1), 29–46. https://doi.org/10.1080/22797254.2017.1274573

Middleton, M., Närhi, P., Sutinen, M., & Sutinen, R. (2008). *Object based change detection of historical aerial photographs reveals altitudinal forest expansion.* https://www.semanticscholar.org/paper/OBJECT-BASED-CHANGE-DETECTION-OF-HISTORICAL-AERIAL-Middleton-N%C3%A4rhi/373b86df6f5979767ef6adbcfcc0b987fa37693f

Mishra, N. B., Mainali, K. P., Shrestha, B. B., Radenz, J., & Karki, D. (2018). Species-Level Vegetation Mapping in a Himalayan Treeline Ecotone Using Unmanned Aerial System (UAS) Imagery. *ISPRS International Journal of Geo-Information*, *7*(11), 445. https://doi.org/10.3390/ijgi7110445

Mohapatra, J., Singh, C. P., Tripathi, O. P., & Pandya, H. A. (2019). Remote sensing of alpine treeline ecotone dynamics and phenology in Arunachal Pradesh Himalaya. *International Journal of Remote Sensing*, *40*(20), 7986–8009. https://doi.org/10.1080/01431161.2019.1608383

Myneni, R. B., Keeling, C. D., Tucker, C. J., Asrar, G., & Nemani, R. R. (1997). Increased plant growth in the northern high latitudes from 1981 to 1991. *Nature*, *386*(6626), 698–702. https://doi.org/10.1038/386698a0

Qiu, L., Jing, L., Hu, B., Li, H., & Tang, Y. (2020). A New Individual Tree Crown Delineation Method for High Resolution Multispectral Imagery. *Remote Sensing*, *12*(3), 585. https://doi.org/10.3390/rs12030585

Ranson, K. J., Montesano, P. M., & Nelson, R. (2011). Object-based mapping of the circumpolar taiga–tundra ecotone with MODIS tree cover. *Remote Sensing of Environment*, *115*(12), 3670–3680. https://doi.org/10.1016/j.rse.2011.09.006

Resler, L. M., Fonstad, M. A., & Butler, D. R. (2004). Mapping the Alpine Treeline Ecotone with Digital Aerial Photography and Textural Analysis. *Geocarto International*, *19*(1), 37–44. https://doi.org/10.1080/10106040408542297

Singh, C. P., Mohapatra, J., & Dharaiya, N. A. (2015). Remote Sensing of alpine Treeline Dynamics. *ISG Newsletter*, *21*(4), 3–8. https://www.researchgate.net/publication/283837476_Remote_Sensing_of_Alpine_Treeline_Dynamics

Stueve, K. M., Isaacs, R. E., Tyrrell, L. E., & Densmore, R. V. (2011). Spatial variability of biotic and abiotic tree establishment constraints across a treeline ecotone in the Alaska

Range. *Ecology*, *92*(2), 496–506. https://doi.org/10.1890/09-1725.1

Virtanen, T., Mikkola, K., Nikula, A., Christensen, J. H., Mazhitova, G. G., Oberman, N. G., & Kuhry, P. (2004). Modeling the Location of the Forest Line in Northeast European Russia with Remotely Sensed Vegetation and GIS-Based Climate and Terrain Data. *Arctic, Antarctic, and Alpine Research*, *36*(3), 314–322. http://www.jstor.org/stable/1552640

Weinstein, B. G., Marconi, S., Bohlman, S. A., Zare, A., & White, E. P. (2020). Cross-site learning in deep learning RGB tree crown detection. *Ecological Informatics*, *56*, 101061. https://doi.org/10.1016/j.ecoinf.2020.101061

Weinstein, B. G., Marconi, S., Bohlman, S., Zare, A., & White, E. (2019). Individual Tree-Crown Detection in RGB Imagery Using Semi-Supervised Deep Learning Neural Networks. *Remote Sensing*, *11*(11), 1309. https://doi.org/10.3390/rs11111309

Whiteside, T. G., Esparon, A. J., & Bartolo, R. E. (2020). A semi-automated approach for quantitative mapping of woody cover from historical time series aerial photography and satellite imagery. *Ecological Informatics*, *55*, 101012. https://doi.org/10.1016/j.ecoinf.2019.101012

Winings, C. J. (2013). Mapping alpine treeline with high resolution imagery and LiDAR data in North Cascades National Park, Washington. *WWU Graduate School Collection*. https://doi.org/https://doi.org/10.25710/9zkh-h696